

Improvement of the Internal Consistency in Trajectory Surface Hopping

Jian-Yun Fang and Sharon Hammes-Schiffer*

Department of Chemistry and Biochemistry, University of Notre Dame, Notre Dame, Indiana 46556-5670

Received: May 17, 1999; In Final Form: July 9, 1999

This paper addresses the issue of internal consistency in the molecular dynamics with quantum transitions (MDQT) surface hopping method. The MDQT method is based on Tully's fewest switches algorithm, which is designed to ensure that the fraction of trajectories on each surface is equivalent to the corresponding average quantum probability determined by coherent propagation of the quantum amplitudes. For many systems, however, this internal consistency is not maintained. Two reasons for this discrepancy are the existence of classically forbidden transitions and the divergence of the independent trajectories. This paper presents a modified MDQT method that improves the internal consistency. The classically forbidden switches are eliminated by utilizing modified velocities for the integration of the quantum amplitudes, and the difficulties due to divergent trajectories are alleviated by removing the coherence of the quantum amplitudes when each trajectory leaves a nonadiabatic coupling region. The standard and modified MDQT methods are compared to fully quantum calculations for a classic model for ultrafast electronic relaxation (i.e., a two-state three-mode model of the conically intersecting S_1 and S_2 excited states of pyrazine). The standard MDQT calculations exhibit significant discrepancies between the fraction of trajectories in each state and the corresponding average quantum probability. The modified MDQT method leads to remarkable internal consistency for this model system.

I. Introduction

Trajectory surface hopping methods have been used extensively to study processes occurring on multiple coupled potential energy surfaces. In these methods the system is divided into a quantum and a classical subsystem. The classical subsystem is approximated as an ensemble of independent trajectories, and each trajectory moves classically on a single potential energy surface with the possibility of instantaneous transitions among the surfaces. The various surface hopping methods^{1–31} differ mainly in how these transitions are incorporated. This paper centers on the molecular dynamics with quantum transitions (MDQT) method, which is based on Tully's stochastic fewest switches algorithm.¹⁴ In this algorithm the quantum amplitudes for all surfaces are propagated coherently along each independent trajectory, and the probability of a transition depends on the rate of change of the quantum probabilities determined from the quantum amplitudes. The number of transitions is minimized by specifying that the flux of trajectories switching from one state to another is unidirectional over a specified time interval. This algorithm is designed to ensure that the fraction of trajectories on each surface is equivalent to the corresponding average quantum probability. As has been noticed in the literature, however, this internal consistency is not always maintained.^{32,33} The goal of this paper is to identify the reasons for this discrepancy and to develop methods for improving the internal consistency of MDQT. These new methods are applied to a model of the conically intersecting S_1 and S_2 excited states of pyrazine. This model system was chosen because it is a classic example of ultrafast electronic relaxation^{34–40} and was previously found to exhibit a significant discrepancy between the fraction of trajectories in each state and the corresponding average quantum probability in MDQT calculations.³³

The reason often cited for the internal inconsistency in MDQT is the existence of classically forbidden transitions. In MDQT, energy is conserved during a transition by adjusting the classical velocities as if they were subjected to a force in the direction of the nonadiabatic coupling vector. If there is not enough velocity in this direction to maintain energy conservation, then the transition is classically forbidden and is not allowed to occur. (In this case, the component of velocity in the direction of the nonadiabatic coupling is reversed¹⁵ or, in some implementations, the velocity is not changed.³³) Such classically forbidden transitions lead to an inconsistency between the fraction of trajectories in each state and the corresponding average quantum probability. The most rigorous way to fix this problem is to increase the size of the quantum mechanical subsystem or to use semiclassical formulations. Unfortunately, a sufficiently large quantum mechanical subsystem is often computationally impractical and, although a number of promising semiclassical formulations have been developed recently,^{41–49} the surface hopping approach is still appealing due to its conceptual simplicity and computational speed.

Classically forbidden transitions can be eliminated in the framework of the MDQT method in a number of ways. One hypothesis is that the forbidden transitions should occur and that the fundamental limitation is the method of velocity adjustment. In this case, classically forbidden transitions can be eliminated by taking energy from other components of the velocities, delaying the transition until the energy is available in the appropriate component of the velocities, or, if all else fails, violating energy conservation. An alternative hypothesis is that the forbidden transitions should not occur and that the fundamental limitation is the method of integrating the quantum amplitudes. In support of this alternative view, Müller and Stock³³ found that for the pyrazine model the agreement with exact quantum calculations was much better for the fraction of

* Corresponding author. E-mail: hammes-schiffer.1@nd.edu.

trajectories in each state than for the corresponding average quantum probability.

Adopting this alternative view, in a previous paper⁵⁰ we presented a modification of MDQT (denoted MDQT*) that eliminates classically forbidden transitions by utilizing modified velocities for the integration of the quantum amplitudes. In this approach, the nonadiabatic coupling between two states vanishes if a switch to the unoccupied state would be classically forbidden. As a result, the quantum amplitudes between these two states are uncoupled so population is not transferred between these two states. According to the fewest switches algorithm, in this case the probability of a transition between these two states vanishes. In ref 50 we applied both MDQT and MDQT* to models representing single and double proton transfer and found that both MDQT and MDQT* maintained internal consistency. In this paper we apply MDQT* to the pyrazine model system to provide a more rigorous test of MDQT*. We show that even in the absence of classically forbidden switches the MDQT* method does not maintain internal consistency for this model system.

Another reason for the lack of internal consistency in MDQT is that the divergence of independent trajectories may lead to a breakdown in the basic assumption of the fewest switches algorithm. This basic assumption is that when a trajectory passes through a nonadiabatic coupling region with nonzero quantum amplitudes for the other surfaces, an ensemble of virtually identical trajectories (i.e., with similar quantum amplitudes and classical coordinates and momenta) are apportioned among the other surfaces according to these quantum amplitudes. (Note that the trajectories are expected to vary slightly due to different initial conditions.) Typically, this assumption is valid for one-dimensional systems involving a single pass through a single nonadiabatic coupling region. Unfortunately, this assumption is violated in many other situations.⁵¹

A dramatic example of the breakdown of the fewest switches algorithm can be illustrated with a two-state model with two nonadiabatic coupling regions. Assume all of the population starts on the upper state, and when it passes through the first nonadiabatic coupling region some of the population transfers down to the lower state. Assume also that there is a barrier on the lower state preventing the lower state population from reaching the second nonadiabatic coupling region. In this case, when the upper state population passes through the second nonadiabatic coupling region the quantum amplitudes of the trajectories are nonzero for the lower state, but there are no trajectories on the lower state in this nonadiabatic coupling region. As a result, the population flux determined by the net change in quantum probabilities for the trajectories on the upper state is inaccurate. (See ref 51 for a clear and comprehensive analysis of such situations.)

A breakdown of the fewest switches algorithm could also occur for a single pass through a single nonadiabatic coupling region if the potential energy surfaces are of very different character in this region (leading to different quantum amplitudes and classical coordinates and momenta of the trajectories on each state). Figure 1 depicts a schematic illustration of such a situation for a two-state model, where P_2 and F_2 indicate the average quantum probability and fraction of trajectories, respectively, for the upper state in an MDQT simulation. As shown in Figure 1a, all of the population is assumed to start on the upper state. As the population passes through the nonadiabatic coupling region, it starts to transfer down to the lower state. If the lower and upper state surfaces are similar throughout the nonadiabatic coupling region, the internal consistency will

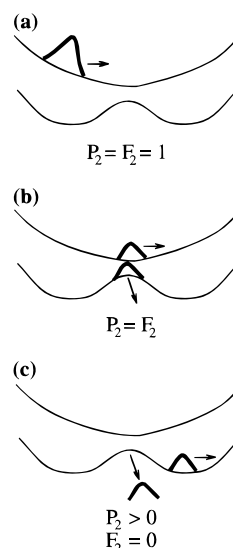


Figure 1. A schematic picture of the effects of divergent trajectories in MDQT simulations, where P_2 and F_2 denote the average quantum probability and the fraction of trajectories, respectively, in the upper state. The populations for the two states are shown for (a) the initial time, (b) an intermediate time, and (c) the final time. The different orientations of the arrows within (b) and (c) indicate that the trajectories are moving in different directions.

be maintained. If the two surfaces differ, however, the trajectories on the lower state may diverge and follow different paths as they leave the nonadiabatic coupling region. In Figure 1, the internal consistency is maintained between the time shown in Figure 1a and the time shown in Figure 1b. The arrows in Figure 1, b and c, indicate that after the time shown in Figure 1b, the trajectories on the lower state move out of the nonadiabatic coupling region before the trajectories on the upper state have passed through the nonadiabatic coupling region. The orientations of the arrows indicate that the trajectories on the lower state are moving in a different direction than those on the upper state. Note that this situation is more likely for multidimensional systems. If the population flux is unidirectional (i.e., from the upper to the lower state) throughout the coupling region, this divergence will not affect the final fraction of trajectories in each state. On the other hand, this divergence will lead to an internal inconsistency because the quantum amplitudes of the divergent trajectories will not be consistent with the quantum amplitudes of the trajectories that continued to move on the excited state. Thus, as illustrated in Figure 1c, the fraction of trajectories on each state may be correct after passing through this nonadiabatic coupling region, but the internal consistency will not be maintained. In this paper we present evidence that this is the main source of the discrepancies noticed by Müller and Stock for the pyrazine model system.

This inconsistency can be alleviated by eliminating the coherence of the quantum amplitudes between well-separated regions of nonadiabatic coupling. In this paper we present a method in which the quantum amplitudes are reset so that the occupied state has a quantum probability of unity after each trajectory has left the nonadiabatic coupling region. (Note that this type of resetting of the quantum amplitudes was also proposed in ref 51. Also note that the resetting of the quantum amplitudes will affect the number of classically forbidden transitions.) We emphasize that resetting the quantum amplitudes is not a general solution to this inherent problem of mixed quantum/classical methods. Clearly this prescription would be inappropriate for systems where the quantum interference between nonadiabatic coupling regions is important.^{29,31} For

many systems, however, such quantum interference effects are washed out due to decoherence in condensed phase systems or averaging over a range of initial conditions. In these cases this method for promoting internal consistency in MDQT is physically justified. We point out that similar methods involving the removal of the coherence of the quantum amplitudes have been applied previously in conjunction with a variety of surface hopping methods.^{4,17,24} Moreover, Rossky and co-workers have performed a thorough analysis of the treatment of coherence in surface hopping.^{52,53}

An outline of this paper is as follows. Section II presents the model system for internal conversion in pyrazine, including the diabatic and adiabatic Hamiltonian matrices for this system. Section III describes the methodology for fully quantum dynamical and mixed quantum/classical MDQT calculations. This section also presents modifications of MDQT to eliminate classically forbidden transitions and to remove the coherence of the quantum amplitudes far from regions of nonadiabatic coupling. Section IV presents the results and compares the various methods, and section V presents our conclusions.

II. Model System

The model system investigated in this paper is a two-state three-mode model of the conical intersection of the $S_1[{}^1B_{3u}(\pi\pi^*)]$ and $S_2[{}^1B_{2u}(\pi\pi^*)]$ excited states of pyrazine. This conical intersection has been shown to trigger an ultrafast $S_2 \rightarrow S_1$ internal conversion process and a dephasing of the vibrational motion on a femtosecond time scale.^{34,36} The model used in this paper includes a single vibronic coupling mode ν_{10a} and two totally symmetric tuning modes ν_1 , ν_{6a} (which modulate the energetic separation of the electronic states). This model invokes the following standard simplifications:^{38,39} (1) the model Hamiltonian is constructed in a diabatic electronic basis; (2) the harmonic approximation is invoked for the diabatic potential energy surfaces and the vibrational frequencies are assumed to be equal for all of the unperturbed surfaces; and (3) interstate and intrastate coupling terms are approximated by linear terms in the normal coordinates. This model has been used throughout the literature as a standard example of ultrafast electronic relaxation.^{34–39} (Note that other models for conical intersections have also been studied with similar methods.⁵⁴)

The Hamiltonian is defined in terms of the two diabatic electronic basis states $|\psi_1^{\text{dia}}\rangle$ and $|\psi_2^{\text{dia}}\rangle$ that represent the two lowest excited singlet states (S_1 and S_2) of pyrazine. The Hamiltonian matrix in the diabatic representation can be expressed as

$$\tilde{\mathbf{H}}^{\text{dia}} = (T_N + V_0)\tilde{\mathbf{I}} + \begin{pmatrix} E_1 + \sum_{j=1}^2 \kappa_j^{(1)} x_j & \lambda x_3 \\ \lambda x_3 & E_2 + \sum_{j=1}^2 \kappa_j^{(2)} x_j \end{pmatrix} \quad (1)$$

In the first term, T_N is the kinetic energy expressed as

$$T_N = \frac{1}{2} \sum_{j=1}^3 \omega_j p_j^2 \quad (2)$$

and V_0 is a harmonic oscillator potential with respect to the electronic ground state equilibrium geometry

$$V_0 = \frac{1}{2} \sum_{j=1}^3 \omega_j x_j^2 \quad (3)$$

Here ω_j is the vibrational frequency and x_j and p_j are the position and momentum of the j th vibrational mode, where $j = 1$ represents the tuning mode ν_1 , $j = 2$ represents the tuning mode ν_{6a} , and $j = 3$ represents the vibronic coupling mode ν_{10a} . For this model the mass corresponding to mode j is $m_j = 1/\omega_j$ with the appropriate units conversion. In this paper the coordinates of the modes are expressed in vector notation as $\mathbf{x} = (x_1, x_2, x_3)$, $\tilde{\mathbf{I}}$ is the identity matrix, and $\hbar = 1$. In the state-dependent part of the Hamiltonian, E_k is the vertical transition energy of the diabatic state k and $\kappa_j^{(k)}$ is the gradient of the excited state potential k with respect to x_j at the ground state equilibrium geometry. The off-diagonal term λx_3 is responsible for the vibronic coupling between the two electronic states. The values of the parameters for this model are given in Table I of ref 33.

Although the diabatic representation is useful for fully quantum dynamical calculations, the adiabatic representation is more appropriate for surface hopping calculations. As shown in ref 55, the transformation from the diabatic to the adiabatic representation is given by

$$\psi^{\text{ad}}(\mathbf{x}) = \tilde{\mathbf{S}}^\dagger(\mathbf{x})\psi^{\text{dia}} \quad (4)$$

where the adiabatic basis states are expressed in vector notation as

$$\psi^{\text{ad}}(\mathbf{x}) = \begin{pmatrix} \psi_1^{\text{ad}}(\mathbf{x}) \\ \psi_2^{\text{ad}}(\mathbf{x}) \end{pmatrix} \quad (5)$$

and the diabatic basis states are expressed in vector notation as

$$\psi^{\text{dia}} = \begin{pmatrix} \psi_1^{\text{dia}} \\ \psi_2^{\text{dia}} \end{pmatrix} \quad (6)$$

The transformation matrix can be expressed as

$$\tilde{\mathbf{S}}(\mathbf{x}) = \begin{pmatrix} \cos \phi & \sin \phi \\ -\sin \phi & \cos \phi \end{pmatrix} \quad (7)$$

where ϕ is defined by

$$\begin{aligned} \sin(2\phi) &= \frac{\lambda x_3}{(\Delta^2 + \lambda^2 x_3^2)^{1/2}} \\ \cos(2\phi) &= \frac{\Delta}{(\Delta^2 + \lambda^2 x_3^2)^{1/2}} \end{aligned} \quad (8)$$

and Δ is half the energy gap between the diabatic electronic surfaces at \mathbf{x} :

$$\Delta = \frac{1}{2} \left[\left(E_2 + \sum_{j=1}^2 \kappa_j^{(2)} x_j \right) - \left(E_1 + \sum_{j=1}^2 \kappa_j^{(1)} x_j \right) \right] \quad (9)$$

Note that the S matrix is a double-valued function of the coordinates \mathbf{x} . In this paper we define a unique S matrix by following the prescription given in ref 56 of setting the signs of S_{11} and S_{22} equal to the sign of x_3 .

Invoking the Born–Oppenheimer approximation, the adiabatic Hamiltonian matrix is

$$\tilde{\mathbf{H}}^{\text{ad}} = (T_N + V_0)\tilde{\mathbf{I}} + \begin{pmatrix} \bar{E} - (\Delta^2 + \lambda^2 x_3^2)^{1/2} & 0 \\ 0 & \bar{E} + (\Delta^2 + \lambda^2 x_3^2)^{1/2} \end{pmatrix} \quad (10)$$

where

$$\bar{E} = \frac{1}{2} \left[\left(E_2 + \sum_{j=1}^2 \kappa_j^{(2)} x_j \right) + \left(E_1 + \sum_{j=1}^2 \kappa_j^{(1)} x_j \right) \right] \quad (11)$$

The two adiabatic Born–Oppenheimer potential energy surfaces are described by

$$W_k(\mathbf{x}) = H_{kk}^{\text{ad}} - T_N \quad (12)$$

(See ref 56 for a discussion of the non-Born–Oppenheimer terms in the adiabatic Hamiltonian.)

III. Methods

A. Fully Quantum Dynamical Method. The fully quantum dynamical calculations were performed in the diabatic representation to avoid numerical difficulties associated with the double-valued nature of the S matrix. The time-dependent wave function $\Psi(\mathbf{x}, t)$ can be expressed in terms of the diabatic basis states as

$$\Psi(\mathbf{x}, t) = \chi_1(\mathbf{x}, t) \psi_1^{\text{dia}} + \chi_2(\mathbf{x}, t) \psi_2^{\text{dia}} \quad (13)$$

where $\chi_k(\mathbf{x}, t)$ is the vibrational wave function corresponding to the diabatic state $|\psi_k^{\text{dia}}\rangle$. Substituting this equation for $\Psi(\mathbf{x}, t)$ into the time-dependent Schrödinger equation using the diabatic Hamiltonian matrix given in eq 10 leads to the two coupled equations of motion

$$\begin{aligned} i\dot{\chi}_1^{\text{dia}}(\mathbf{x}, t) &= V_{11}(\mathbf{x})\chi_1^{\text{dia}}(\mathbf{x}, t) + V_{12}(\mathbf{x})\chi_2^{\text{dia}}(\mathbf{x}, t) \\ i\dot{\chi}_2^{\text{dia}}(\mathbf{x}, t) &= V_{21}(\mathbf{x})\chi_1^{\text{dia}}(\mathbf{x}, t) + V_{22}(\mathbf{x})\chi_2^{\text{dia}}(\mathbf{x}, t) \end{aligned} \quad (14)$$

where V_{ij} are matrix elements of the matrix $\tilde{\mathbf{H}}^{\text{dia}} - T_N \tilde{\mathbf{I}}$. We solve these equations of motion using the predictor–corrector method with the discrete variable representation. These results are converted to the adiabatic representation for comparison to the surface hopping results using the projector operator defined in ref 55.

B. Surface Hopping Methods. 1. Standard MDQT Method. In surface hopping methods the classical subsystem moves according to the standard classical equations of motion

$$m_j \ddot{x}_j = - \frac{\partial W_k(\mathbf{x})}{\partial x_j} \quad (15)$$

where $W_k(\mathbf{x})$ (defined in eq 12) is the potential energy of the occupied adiabatic state. The time-dependent wave function describing the quantum mechanical state at time t is expanded in terms of the two adiabatic states

$$\Psi(\mathbf{x}, t) = C_1(t) \psi_1^{\text{ad}}(\mathbf{x}) + C_2(t) \psi_2^{\text{ad}}(\mathbf{x}) \quad (16)$$

where $C_i(t)$ are complex-valued expansion coefficients (i.e., quantum amplitudes). Note that the adiabatic states are also time-dependent through the classical trajectory $\mathbf{x}(t)$. Substitution of the wave function $\Psi(\mathbf{x}, t)$ into the time-dependent Schrödinger equation using the adiabatic Hamiltonian matrix $\tilde{\mathbf{H}}^{\text{ad}}$ given in eq 10 leads to the following equations of motion for the quantum amplitudes:

$$\dot{C}_k = -iC_k W_k - \sum_{j=1}^2 C_j \dot{\mathbf{x}} \cdot \mathbf{d}_{kj} \quad (17)$$

where $\dot{\mathbf{x}}$ denotes the time derivatives of the coordinates \mathbf{x} and \mathbf{d}_{kj} is the nonadiabatic coupling vector defined as

$$\mathbf{d}_{kj} = \langle \psi_k^{\text{ad}} | \nabla_{\mathbf{x}} \psi_j^{\text{ad}} \rangle = \sum_{i=1}^2 S_{ik} \nabla_{\mathbf{x}} S_{ij} \quad (18)$$

for $j \neq k$ and $\mathbf{d}_{kk} = 0$. In density matrix notation, the density matrix elements are defined as $a_{kj} = C_k C_j^*$, where the diagonal density matrix elements a_{kk} are the occupation probabilities of the adiabatic states, and the off-diagonal elements a_{kj} describe the coherence. In practice, eqs 15 and 17 are integrated numerically to simultaneously propagate the coordinates and momenta (\mathbf{x} , \mathbf{p}) and the quantum amplitudes C_j .

The surface hopping calculations in this paper are based on the molecular dynamics with quantum transitions (MDQT) surface hopping method.^{14,15} The MDQT method implements Tully's fewest switches algorithm,¹⁴ which is designed to correctly apportion trajectories among the states according to the quantum probabilities $|C_j(t)|^2$ with the minimum required number of quantum transitions. In this algorithm the probability of switching states is defined in terms of the rate of change of the occupation probabilities, which can be derived from eq 17 to be

$$\dot{a}_{kk} = \sum_{j \neq k} b_{kj} \quad (19)$$

where

$$b_{jk} = -2\text{Re}(a_{jk}^* \dot{\mathbf{x}} \cdot \mathbf{d}_{jk}) \quad (20)$$

The rate of change of the occupation probability for state k due to coupling with state j is b_{kj} , so the change in the occupation probability for state k due to coupling with state j over a short time interval δt is $b_{kj} \delta t$. The number of state switches is minimized by assuming that the flux of probability between each pair of states results from probability transferring in only one direction. According to this algorithm, the probability of switching from the current state k to another state j during the time interval between t and $t + \delta t$ is

$$g_{kj}(t, \delta t) = \max\left(0, \frac{b_{jk} \delta t}{a_{kk}}\right) \quad (21)$$

where b_{jk} and a_{kk} are assumed to remain approximately constant during the short time interval δt and thus can be evaluated either at time t or at time $t + \delta t$. If $b_{jk} < 0$ then the occupation probability of the occupied state k can be viewed as increasing due to coupling with state j , so the probability of switching from state k to state j is zero. On the other hand, if $b_{jk} > 0$ then the occupation probability of the occupied state k can be viewed as decreasing due to coupling with state j , so the probability of switching from state k to state j is $b_{jk} \delta t / a_{kk}$. References 14 and 22 illustrate that this algorithm achieves the correct statistical populations of the states for model systems.

In order to determine whether a switch to any state j will occur, a uniform random number ξ ($0 < \xi < 1$) is selected at each time step in the trajectory. For example, for a two-state system, if the occupied state $k = 1$ then a switch to state 2 will occur if $\xi < g_{12}$. If a switch to a different state j does occur and if $W_k \neq W_j$, then the velocities must be adjusted in order to conserve total energy. The velocities should be adjusted as if they were subjected to a force in the direction of the nonadiabatic coupling vector.¹⁴ As derived in ref 15, the new velocities $\dot{\mathbf{x}}'$

can be calculated as follows:

$$\dot{x}'_i = \dot{x}_i - \gamma_{kj} d_{kj}^i / m_i \quad (22)$$

where d_{kj}^i specifies the i th component of the three-dimensional vector \mathbf{d}_{kj} , and

$$\gamma_{kj} \equiv \frac{\beta_{kj} + \sqrt{\beta_{kj}^2 + 4\alpha_{kj}[W_k(\mathbf{x}) - W_j(\mathbf{x})]}}{2\alpha_{kj}}, \quad \beta_{kj} < 0 \quad (23)$$

$$\gamma_{kj} \equiv \frac{\beta_{kj} - \sqrt{\beta_{kj}^2 + 4\alpha_{kj}[W_k(\mathbf{x}) - W_j(\mathbf{x})]}}{2\alpha_{kj}}, \quad \beta_{kj} \geq 0 \quad (24)$$

where

$$\alpha_{kj} \equiv \frac{1}{2} \sum_{i=1}^3 m_i^{-1} (d_{kj}^i)^2 \quad (25)$$

and

$$\beta_{kj} \equiv \sum_{i=1}^3 \dot{x}_i d_{kj}^i \quad (26)$$

Note that a switch can occur only if

$$\beta_{kj}^2 + 4\alpha_{kj}[W_k(\mathbf{x}) - W_j(\mathbf{x})] \geq 0 \quad (27)$$

Otherwise, there is not enough velocity in the direction of the nonadiabatic coupling vector to maintain energy conservation, and the system remains in the initial quantum state. This situation is denoted a classically forbidden transition. Within the framework of standard MDQT, there are two different approaches for determining the velocities after classically forbidden transitions. In the first approach, the component of velocity in the direction of the nonadiabatic coupling vector is reversed; i.e., the velocities are changed according to eq 22 with $\gamma_{kj} = \beta_{kj}/\alpha_{kj}$.¹⁵ In the second approach, the velocities are not adjusted.³³ In either approach, these classically forbidden transitions lead to inconsistencies between the fraction of trajectories $F_i(t)$ in each state i and the corresponding average quantum probability $\langle |C_i(t)|^2 \rangle$.

2. MDQT* Method for Eliminating Classically Forbidden Switches. Recently we presented a modified MDQT method (denoted MDQT*) originally proposed by Tully⁵⁷ to eliminate classically forbidden transitions. In MDQT* the quantum amplitudes are integrated using modified velocities $\dot{\mathbf{x}}_{ij}$:

$$\dot{C}_i = -iC_i W_i - \sum_{j=1}^2 C_j \dot{\mathbf{x}}_{ij} \cdot \mathbf{d}_{ij} \quad (28)$$

and the velocity $\dot{\mathbf{x}}_{jk}$ replaces $\dot{\mathbf{x}}$ in eq 20 for the calculation of b_{jk} used to calculate the probability of switching from state k to state j . The modified velocities are defined as

$$\dot{\mathbf{x}}_{ij} = \sqrt{\dot{x}'_i \dot{x}'_j} \frac{\dot{\mathbf{x}}}{\dot{x}} \quad (29)$$

where $\dot{\mathbf{x}}$ is the classical velocity for the occupied state k , and \dot{x}'_i , \dot{x}'_j , and \dot{x} are the magnitudes of the three-dimensional vectors $\dot{\mathbf{x}}'_i$, $\dot{\mathbf{x}}'_j$, and $\dot{\mathbf{x}}$, respectively. (Note that $\dot{\mathbf{x}}_{ij} = \dot{\mathbf{x}}_{ji}$.)

In this paper we examine two different approaches for defining the modified velocities within the framework of MDQT*. In both approaches, $\dot{x}'_j = 0$ if a switch from the

occupied state k to state j would be classically forbidden (i.e., if eq 27 is not satisfied). Otherwise, in the first approach $\dot{\mathbf{x}}'_j$ is the velocity that would be obtained using the prescription in eq 22 to conserve total energy for a transition from the occupied state k to state j , and in the second approach $\dot{\mathbf{x}}'_j = \dot{\mathbf{x}}$. (Note that in both approaches $\dot{\mathbf{x}}'_k = \dot{\mathbf{x}}$.) In both MDQT* approaches, if a hop from state k to state j would be classically forbidden, the nonadiabatic coupling between states k and j vanishes (i.e., all components of $\dot{\mathbf{x}}_{kj}$ are zero) so the flux of quantum probability from state k to state j vanishes (i.e., $b_{jk} = 0$). According to the fewest switches algorithm, in this case the probability of switching from state k to state j is zero (i.e., $g_{kj} = 0$). Thus, the classically forbidden transitions are eliminated.

We emphasize that MDQT* is not based on rigorous theoretical grounds, but rather is a minor modification that eliminates the classically forbidden transitions while maintaining the appealing simplicity and computational speed of MDQT. MDQT* is the same as MDQT in that the classical subsystem moves according to standard classical equations of motion using the positions \mathbf{x} and velocities $\dot{\mathbf{x}}$ on the occupied state k . Moreover, MDQT and MDQT* use the same fewest switches algorithm and the same method for scaling velocities after a state switch to conserve total energy. MDQT* differs from MDQT only in the integration of the quantum amplitudes, which invokes the modified velocities. In the first MDQT* approach, the modified velocities are geometric averages of the velocities in different states. In the second MDQT* approach, the modified velocities are identical to the standard velocity used in MDQT (i.e., the velocity for the occupied state) except that the modified velocity is set to zero if a transition would be classically forbidden. The second MDQT* approach is more appealing in that it is identical to standard MDQT in the absence of classically forbidden transitions. In both MDQT* approaches, however, MDQT* is virtually identical to MDQT far from the nonadiabatic coupling region (since the nonadiabatic coupling vanishes) and in the strong coupling region (since the energy difference between the coupled states is so small that the velocity adjustment due to a transition would be negligible). Furthermore, the results in ref 50 and in this paper indicate that the MDQT and MDQT* methods lead to virtually identical adiabatic populations (determined by the fraction of trajectories in each adiabatic state) for a variety of model systems.

3. Removal of Coherence of the Quantum Amplitudes. As discussed in the Introduction, even in the absence of classically forbidden switches, the fewest switches algorithm does not always maintain consistency between the fraction of trajectories $F_i(t)$ and the average quantum probability $\langle |C_i|^2 \rangle$. In standard MDQT the quantum amplitudes are propagated coherently throughout each trajectory. When independent trajectories diverge, this coherent propagation may lead to an inconsistency between the fraction of trajectories in each state and the corresponding average quantum probability. This internal inconsistency can be improved if the quantum amplitudes are reset so that the quantum amplitude of the occupied state is unity after passing through a nonadiabatic coupling region. In this paper the quantum amplitudes are reset when the magnitude of the nonadiabatic coupling vector $|\mathbf{d}_{12}|$ between the two adiabatic states becomes smaller than a specified tolerance. Clearly this resetting of the quantum amplitudes is not appropriate for systems where the quantum interference between nonadiabatic coupling regions is important.^{29,31} This resetting of the quantum amplitudes is physically justified, however, if the quantum interference effects between the nonadiabatic coupling regions are washed out by decoherence effects or by

averaging over a range of initial conditions. In this paper the resetting of the quantum amplitudes is used as a numerical tool to correct a deficiency of the MDQT method.

C. Initial Conditions. The fully quantum calculations were performed in the diabatic representation. In this case, the initial wavepacket is a Gaussian wavepacket on the second diabatic electronic state:

$$\begin{aligned}\psi_1^{\text{dia}}(\mathbf{x}) &= 0 \\ \psi_2^{\text{dia}}(\mathbf{x}) &= A \exp[-1/2(x_1^2 + x_2^2 + x_3^2)]\end{aligned}\quad (30)$$

where A is a normalization factor. Note that the exponential also includes a units conversion factor from use of the identity $\omega_j m_j = 1$.

The MDQT calculations were performed in the adiabatic representation. In this case, the initial conditions for the nuclear variables were obtained from classical action-angle variables;^{33,58}

$$\begin{aligned}x_j(0) &= \sin \alpha_j \\ p_j(0) &= \cos \alpha_j\end{aligned}\quad (31)$$

where the angles α_j are randomly picked from the interval $[0, 2\pi]$. Again, these expressions include a units conversion factor from use of the identity $\omega_j m_j = 1$. Note that these initial conditions were chosen to allow direct comparison to the results in ref 33. Discrepancies between the fully quantum and MDQT initial conditions for the nuclear variables may be responsible for small differences between the MDQT and fully quantum calculations. The initial conditions for the quantum probabilities in the adiabatic representation were obtained by applying the projection operator defined in ref 55 to the initial wavepacket in the diabatic representation. The fraction of trajectories starting in each adiabatic state was chosen to be consistent with these quantum probabilities, and the phases of the initial quantum amplitudes were set to zero. 5000 trajectories were propagated with a time step of 0.012 fs for each calculation.

IV. Results

In this section we present the results of the application of the methods discussed in section III to the model system for internal conversion in pyrazine described in section II. Figure 2 depicts the time evolution of the population (i.e., the occupation probability) of the upper adiabatic state. For the fully quantum results we plot $\int d\mathbf{x} |\psi_2^{\text{ad}}(\mathbf{x}, t)|^2$, and for the surface hopping results we plot both the average quantum probability $\langle |C_2(t)|^2 \rangle$ and the fraction of trajectories $F_2(t)$. The fully quantum results are shown with solid lines and the surface hopping results are shown with dashed lines. In all cases the population of the upper adiabatic state exhibits an ultrafast initial decay within less than 50 fs, followed by a number of weak recurrences.

Figure 2a,b depicts the results of the standard MDQT method, where in Figure 2a the component of velocity in the direction of the nonadiabatic coupling vector is reversed after a classically forbidden transition and in Figure 2b the velocities are not altered after a classically forbidden transition. In both cases the fraction of trajectories in the upper state for the MDQT calculations agrees qualitatively with the fully quantum results. As shown previously,³³ the quantitative agreement is better for the algorithm in which the velocities are not adjusted after classically forbidden transitions. In particular, for the results with velocity reversal (Figure 2a), the first few recurrences are

weaker, and the recurrences are completely damped out at later times. In both MDQT methods, however, the quantum probability does not agree well with the fraction of trajectories, indicating a significant internal inconsistency.

As discussed in the Introduction, the reason most often cited for this lack of internal consistency in MDQT is the existence of classically forbidden transitions. Figure 3 depicts the time evolution of the total number of classically forbidden transitions for 5000 trajectories (corresponding to the results in Figure 2b). The classically forbidden transitions start to occur at ~ 5 fs and continue to occur at a constant rate of 0.02 fs⁻¹ per trajectory (i.e., 2% of the trajectories exhibit a classically forbidden transition each femtosecond). The absence of a significant number of classically forbidden transitions before ~ 5 fs is due to the use of initial conditions with 96% of the trajectories starting on the upper state. (All transitions from the upper to the lower state are allowed.) The substantial number of classically forbidden switches occurring after ~ 5 fs suggests that this may be a cause of the internal inconsistency in these calculations. On the other hand, the number of classically forbidden transitions increases at a constant rate, whereas the discrepancy between the quantum probability and the fraction of trajectories becomes virtually constant after 200 fs. This observation suggests that the classically forbidden transitions may not be the main cause of this discrepancy.

To determine the degree to which the classically forbidden transitions are responsible for the significant internal inconsistency illustrated in Figure 2a,b, we applied the MDQT* method to this model system. Figure 2, c and d, depicts the results of the standard MDQT* method using the two different prescriptions discussed in section III. The results are virtually identical for the two different prescriptions and are similar to the results of Figure 2b. The quantum probability still does not agree well with the fraction of trajectories for the MDQT* method. Thus, these results indicate that the classically forbidden transitions are not responsible for the large internal inconsistency.

As discussed in the Introduction, another cause of internal inconsistency is the divergence of the independent trajectories in the ensemble, which may lead to a breakdown of the basic assumption of the fewest switches algorithm. If the independent trajectories diverge while the ensemble is passing through the nonadiabatic coupling region and the flux of population is predominantly unidirectional throughout this region, the fraction of trajectories in each state could be accurate while the average quantum probabilities are inconsistent. In support of this hypothesis, Figure 4 depicts the distribution of quantum probabilities $|C_2(t)|^2$ after the ensemble has first passed through the nonadiabatic coupling region ($t = 67.7$ fs) for the calculations shown in Figure 2d. Although $\sim 30\%$ of the trajectories have a quantum probability less than 0.1, the remaining trajectories have quantum probabilities ranging from 0.1 to 0.95. These trajectories must have followed divergent paths when the ensemble passed through the region of nonadiabatic coupling. As a result, their quantum amplitudes are not representative of the ensemble.

This source of the internal inconsistency can be eliminated by removing the coherence of the quantum amplitudes when each trajectory leaves the nonadiabatic coupling region. As discussed in section III, in our calculations the criterion for resetting the quantum amplitudes to unity for the occupied state is the magnitude of the nonadiabatic coupling vector $|\mathbf{d}_{12}|$ becoming less than a specified tolerance. In our calculations, we used a tolerance of 0.1 au. To justify this choice, Figure 5 depicts the magnitude of the nonadiabatic coupling vector for

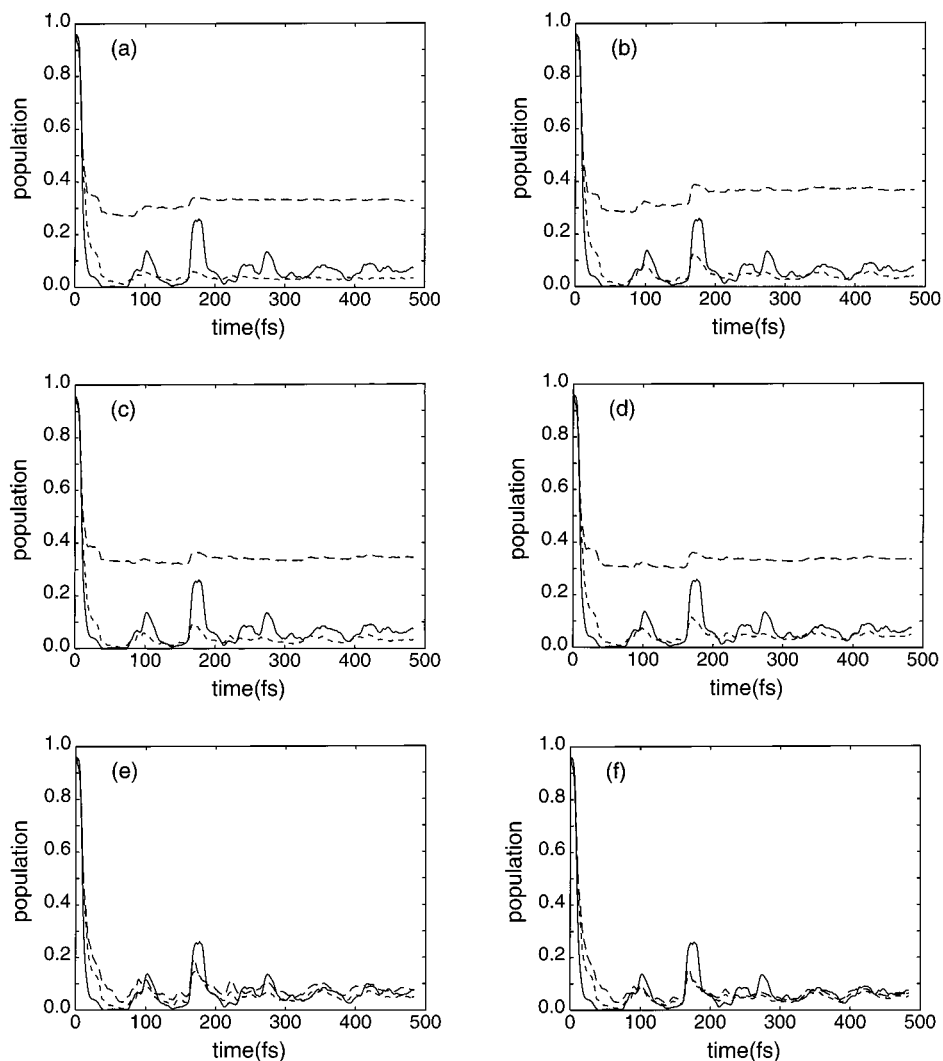


Figure 2. Time evolution of the population (i.e., the occupation probability) of the upper adiabatic state for fully quantum and surface hopping calculations. The fully quantum results depict $\int dx |\psi_2^{\text{ad}}(\mathbf{x}, t)|^2$ (solid line), and the surface hopping results depict both the average quantum probability $\langle |C_2(t)|^2 \rangle$ (long dashed line) and the fraction of trajectories $F_2(t)$ (short dashed line). (a) Standard MDQT with the component of velocity in the direction of the nonadiabatic coupling vector reversed after classically forbidden transitions; (b) standard MDQT with no modification of the velocities after classically forbidden transitions; (c) standard MDQT* with the modified velocity defined such that \dot{x}'_j (used in eq 29) is set to zero if a transition to state j would be classically forbidden and to the magnitude of the velocity that would be obtained by conserving total energy after a transition to state j otherwise; (d) standard MDQT* with the modified velocity defined such that \dot{x}'_j (used in eq 29) is set to zero if a transition to state j would be classically forbidden and to \dot{x} otherwise; (e) MDQT method of Figure 2b with quantum amplitudes reset so that the quantum probability of the occupied state is unity when $|\mathbf{d}_{12}| < 0.1$ au; (f) MDQT* method of Figure 2d with quantum amplitudes reset so that the quantum probability of the occupied state is unity when $|\mathbf{d}_{12}| < 0.1$ au.

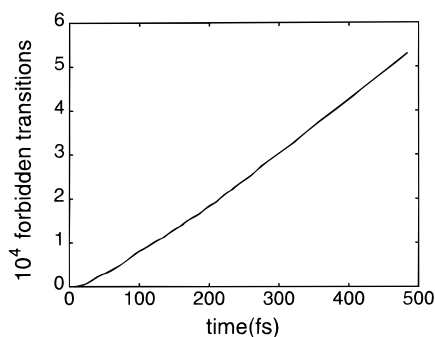


Figure 3. Time evolution of the total number of classically forbidden transitions for the 5000 MDQT trajectories corresponding to Figure 2b.

three representative trajectories. Note that the tolerance was chosen to be close to the minimum value of $|\mathbf{d}_{12}|$ for these representative trajectories. Figure 2, e and f, depicts the results of the MDQT and MDQT* methods (corresponding to Figure

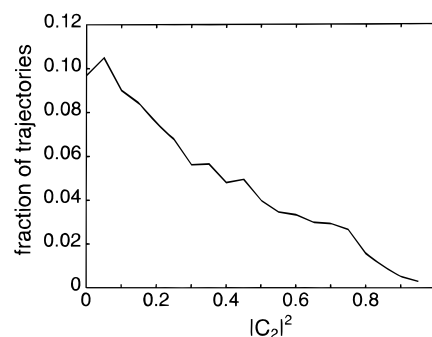


Figure 4. A normalized distribution of the quantum probabilities at time $t = 67.7$ fs for the MDQT* results shown in Figure 2d.

2, b and d) with the coherence removed using this method. In this case, the quantum probability agrees extremely well with the fraction of trajectories. We emphasize that the resetting of the quantum amplitudes enforces the internal consistency by construction. As shown in Figure 2, however, this resetting of

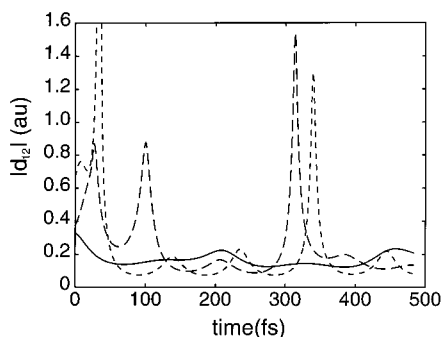


Figure 5. Time evolution of the magnitude of the nonadiabatic coupling vector $|d_{12}|$ for three representative MDQT* trajectories corresponding to Figure 2d. The solid curve corresponds to a trajectory that started on the lower adiabatic state, and the dashed curves correspond to trajectories that started on the upper adiabatic state.

the quantum amplitudes not only improves the internal consistency but also slightly improves the agreement between the surface hopping and the exact quantum results for the adiabatic populations.

These results indicate that the internal inconsistency is due mainly to the breakdown of the fewest switches algorithm resulting from diverging trajectories. On the other hand, a comparison of Figure 2, e and f, indicates that the internal consistency is better for MDQT* than for MDQT. Specifically, the value of the difference between the quantum probability and the fraction of trajectories averaged over times greater than 100 fs is 0.011 for MDQT* (Figure 2f) and 0.024 for MDQT (Figure 2e). Thus, the elimination of classically forbidden switches is also a significant aspect of maintaining internal consistency.

V. Conclusions

In this paper we identified two reasons for discrepancies between the fraction of trajectories in each state and the corresponding average quantum probability in MDQT calculations. One reason for this discrepancy is the existence of classically forbidden transitions. Another reason for this discrepancy is that divergence of the independent trajectories may lead to a breakdown of the basic assumption of the fewest switches algorithm. We presented modifications of MDQT to improve the internal consistency. In these methods the classically forbidden switches are eliminated by using modified velocities for the integration of the quantum amplitudes, and the difficulties due to divergent trajectories are alleviated by removing the coherence of the quantum amplitudes when each trajectory leaves the nonadiabatic coupling region. We compared the standard and modified MDQT methods to fully quantum calculations for a classic model for ultrafast electronic relaxation (i.e., a two-state three-mode model of the conically intersecting S_1 and S_2 excited states of pyrazine). For this model, the standard MDQT calculations exhibited significant discrepancies between the fraction of trajectories in each state and the corresponding average quantum probability. Our results indicate that for this model the divergence of independent trajectories is mainly responsible for this large internal inconsistency, although the classically forbidden transitions also cause minor discrepancies. The modified MDQT method improving both aspects resulted in remarkable internal consistency for this model system. Thus, this modified MDQT method should be useful for future surface hopping calculations on similar systems that are vibronically coupled through a conical intersection.

Surface hopping methods such as MDQT are appealing due to their conceptual simplicity and computational speed. Com-

parisons of MDQT to fully quantum calculations for simple one-dimensional model systems illustrate the potential accuracy of these methods.^{14,24,25} On the other hand, surface hopping methods have been shown to be inaccurate for certain types of systems.^{27–29} For example, surface hopping methods are problematic for processes involving an extended nonadiabatic coupling region or a large number of successive recrossings of a nonadiabatic coupling region.^{29,31} Moreover, surface hopping methods are not appropriate when tunneling of the classical degrees of freedom is important (i.e., for processes involving classically treated reacting H atoms). To determine when surface hopping methods are accurate, these methods should be compared to fully quantum results for a wide range of different types of models. Future work will center on testing the modified MDQT method presented in this paper for other model systems to determine the extent of its applicability.

Acknowledgment. We gratefully acknowledge useful discussions with John Tully about surface hopping methods and with Gerhard Stock about the model system studied in this paper. In addition, we acknowledge financial support from the AFOSR Grant No. F49620-98-1-0209 and the NSF Grant No. CHE-9623813. S.H.S. is a recipient of an Alfred P. Sloan Foundation Research Fellowship and a Camille Dreyfus Teacher Scholar Award.

References and Notes

- (1) Tully, J. C.; Preston, R. K. *J. Chem. Phys.* **1971**, *55*, 562.
- (2) Miller, W. H.; George, T. F. *J. Chem. Phys.* **1972**, *56*, 5637.
- (3) Stine, J. R.; Muckerman, J. T. *J. Chem. Phys.* **1976**, *65*, 3975.
- (4) Blais, N. C.; Truhlar, D. G. *J. Chem. Phys.* **1983**, *79*, 1334.
- (5) Dunne, L. J.; Murrell, J. N.; Stamper, J. G. *Chem. Phys. Lett.* **1984**, *112*, 497.
- (6) Parlant, G.; Gislason, E. A. *J. Chem. Phys.* **1989**, *91*, 4416.
- (7) Parlant, G.; Alexander, M. H. *J. Chem. Phys.* **1990**, *92*, 2287.
- (8) Kuntz, P. J. *J. Chem. Phys.* **1991**, *95*, 141.
- (9) Kuntz, P. J.; Hogreve, J. J. *J. Chem. Phys.* **1991**, *95*, 156.
- (10) Herman, M. F. *J. Chem. Phys.* **1984**, *81*, 754.
- (11) Herman, M. F. *J. Chem. Phys.* **1984**, *81*, 764.
- (12) Herman, M. F.; Arce, J. C. *Chem. Phys.* **1994**, *183*, 335.
- (13) Arce, J. C.; Herman, M. F. *J. Chem. Phys.* **1994**, *101*, 7520.
- (14) Tully, J. C. *J. Chem. Phys.* **1990**, *93*, 1061.
- (15) Hammes-Schiffer, S.; Tully, J. C. *J. Chem. Phys.* **1994**, *101*, 4657.
- (16) Webster, F. J.; Schnitker, J.; Friedrichs, M. S.; Friesner, R.; Rossky, P. *Phys. Rev. Lett.* **1991**, *66*, 3172.
- (17) Webster, F.; Rossky, P. J.; Friesner, R. A. *Comput. Phys. Commun.* **1991**, *63*, 494.
- (18) Webster, F.; Wang, E. T.; Rossky, P. J.; Friesner, R. A. *J. Chem. Phys.* **1994**, *100*, 4835.
- (19) Space, B.; Coker, D. F. *J. Chem. Phys.* **1991**, *94*, 1976.
- (20) Space, B.; Coker, D. F. *J. Chem. Phys.* **1992**, *96*, 652.
- (21) Coker, D. F.; Xiao, L. *J. Chem. Phys.* **1995**, *102*, 496.
- (22) Coker, D. F. In *Computer Simulation in Chemical Physics*; Allen, M. P., Tildesley, D. J., Eds.; Kluwer Academic: Dordrecht, 1993; p 315.
- (23) Prezhdo, O. V.; Rossky, P. J. *J. Chem. Phys.* **1997**, *107*, 825.
- (24) Morelli, J.; Hammes-Schiffer, S. *Chem. Phys. Lett.* **1997**, *269*, 161.
- (25) Fang, J.-Y.; Hammes-Schiffer, S. *J. Chem. Phys.* **1997**, *107*, 8933.
- (26) Hammes-Schiffer, S. *J. Phys. Chem. A* **1998**, *102*, 10443.
- (27) Topaler, M. S.; Allison, T. C.; Schwenke, D. W.; Truhlar, D. G. *J. Phys. Chem. A* **1998**, *102*, 1666.
- (28) Topaler, M. S.; Allison, T.; Schwenke, D. W.; Truhlar, D. G. *J. Chem. Phys.* **1998**, *109*, 3321.
- (29) Kohen, D.; Stillinger, F. H.; Tully, J. C. *J. Chem. Phys.* **1998**, *109*, 4713.
- (30) Sholl, D. S.; Tully, J. C. *J. Chem. Phys.* **1998**, *109*, 7702.
- (31) Tully, J. C. *Faraday Discuss.* **1998**, *110*, 407.
- (32) Neria, E.; Nitzan, A. *J. Chem. Phys.* **1993**, *99*, 1109.
- (33) Müller, U.; Stock, G. *J. Chem. Phys.* **1997**, *107*, 6230.
- (34) Schneider, R.; Domcke, W. *Chem. Phys. Lett.* **1988**, *150*, 235.
- (35) Stock, G.; Schneider, R.; Domcke, W. *J. Chem. Phys.* **1989**, *90*, 7184.
- (36) Schneider, R.; Domcke, W.; Koppel, H. *J. Chem. Phys.* **1990**, *92*, 1045.
- (37) Stock, G. *J. Chem. Phys.* **1995**, *103*, 2888.
- (38) Prasad, M. D. *Chem. Phys. Lett.* **1992**, *194*, 27.

- (39) Latha, G. S.; Prasad, M. D. *J. Chem. Phys.* **1996**, *105*, 2972.
(40) Stock, G.; Woywod, C.; Domcke, W.; Swinney, T.; Hudson, B. S. *J. Chem. Phys.* **1995**, *103*, 6851.
(41) Herman, M. F. *J. Chem. Phys.* **1995**, *103*, 8081.
(42) Martinez, T. J.; Ben-Nun, M.; Levine, R. D. *J. Phys. Chem.* **1996**, *100*, 7884.
(43) Sun, X.; Miller, W. H. *J. Chem. Phys.* **1997**, *106*, 6346.
(44) Xiong, S.; Haobin, W.; Miller, W. H. *J. Chem. Phys.* **1998**, *109*, 7064.
(45) Haobin, W.; Song, X.; Chandler, D.; Miller, W. H. *J. Chem. Phys.* **1999**, *110*, 4824.
(46) Herman, M. F. *Int. J. Quantum Chem.* **1998**, *70*, 897.
(47) Herman, M. F. *J. Chem. Phys.* **1999**, *110*, 4141.
(48) Ben-Nun, M.; Martinez, T. *J. Chem. Phys.* **1998**, *108*, 7244.
(49) Ben-Nun, M.; Martinez, T. *J. Chem. Phys.* **1999**, *110*, 4134.
(50) Fang, J.-Y.; Hammes-Schiffer, S. *J. Chem. Phys.* **1999**, *110*, 11166.
(51) Thachuk, M.; Ivanov, M. Y.; Wardlaw, D. M. *J. Chem. Phys.* **1998**, *109*, 5747.
(52) Bittner, E. R.; Rossky, P. J. *J. Chem. Phys.* **1995**, *103*, 8130.
(53) Schwartz, B. J.; Bittner, E. R.; Prezhdo, O. V.; Rossky, P. J. *J. Chem. Phys.* **1996**, *104*, 5942.
(54) Cattaneo, P.; Persico, M. *J. Phys. Chem. A* **1997**, *101*, 3454.
(55) Manthe, U.; Koppel, H. *J. Chem. Phys.* **1990**, *93*, 345.
(56) Koppel, H.; Domcke, W.; Cederbaum, L. S. *Adv. Chem. Phys.* **1984**, *57*, 59.
(57) Tully, J. C., private communication.
(58) Child, M. S. *Theory of Chemical Reaction Dynamics*; CRC Press: Boca Raton, FL, 1985; Vol. III.